Improving the joint estimation of CO₂ and surface carbon fluxes using a Constrained Ensemble Kalman Filter in COLA (v1.0)

Zhiqiang Liu[1,2], Ning Zeng[3,4,1], Yun Liu[5,6], Eugenia Kalnay[3], Ghassem Asrar[7], Bo Wu[1], Qixiang Cai[1], Di Liu[8], Pengfei Han[9,1]

[1]State Key Laboratory of Numerical Modeling for Atmospheric Sciences and Geophysical Fluid Dynamics, Institute of Atmospheric Physics, Chinese Academy of Sciences, Beijing, China
[2]College of Earth and Planetary Sciences, University of Chinese Academy of Sciences, Beijing, China
[3]Dept. of Atmospheric and Oceanic Science, University of Maryland – College Park, Maryland, USA
[4]Earth System Science Interdisciplinary Center, University of Maryland, USA
[5]International Laboratory for High-Resolution Earth System Model and Prediction (iHESP), Texas A&M University, College Station, Texas, USA
[6]Dept. of Oceanography, Texas A & M University, College Station, TX, USA
[7]Universities Space Research Association, Columbia, MD, USA
[8]Research Center for Eco-Environmental Sciences, Chinese Academy of Sciences, Beijing, China
[9]Carbon Neutrality Research Center, Institute of Atmospheric Physics, Chinese Academy of Sciences, Beijing, China

Correspondence to: Zhiqiang Liu (liuzhiqiang@mail.iap.ac.cn) and Ning Zeng (zeng@umd.edu)

Abstract. Atmospheric inversion of carbon dioxide (CO₂) measurements to understand carbon sources and sinks has made great progress over the last two decades. However, most of the studies, including four-dimension variational (4D-Var), Ensemble Kalman filter (EnKF), and Bayesian synthesis approaches, obtains directly only fluxes while CO₂ concentration is derived with the forward model as post-analysis. Kang et al. (2012) used the Local Ensemble Transform Kalman Filter (LETKF) that updates the CO₂, surface carbon fluxes (SCF), and meteorology field simultaneously. Following this track, a system with a short assimilation window and a long observation window was developed (Liu et al., 2019). However, this system faces the challenge of maintaining global carbon mass. To overcome this shortcoming, here we introduce a Constrained Ensemble Kalman Filter (CEnKF) approach to ensure the conservation of global CO₂ mass. After a standard LETKF procedure, an additional assimilation process is applied to adjust CO₂ at each model grid point and to ensure the consistency between the analysis and the first guess of global CO₂ mass. In the context of observing system simulation experiments (OSSEs), we show that the CEnKF can significantly reduce the annual global SCF bias from ~0.2 gigaton to less than 0.06 gigaton by comparing between experiments with and without it. Moreover, the annual bias over most continental regions is also reduced. At the seasonal scale, the improved system reduced the flux root-mean-square error from priori to analysis by 48-90%, depending on the continental region. Moreover, the 2015-2016 El Nino impact is well captured with anomalies mainly in the tropics.

1 Introduction

Carbon dioxide (CO₂) plays a crucial role in climate system and its projected warming (Friedlingstein et al., 2006). About half of the fossil fuel and cement emissions are absorbed by the land and ocean, leaving the remaining half in the atmosphere

(Friedlingstein et al., 2019). Without effective reduction of those emissions and advanced technologies for carbon capture and
35 storage, the warming trend may exceed the tipping point with potential adverse impacts on the health of environment, people,
and global economy. Recently, many countries (e.g., Asian, European, and North and South American countries) announced
their pledge for achieving carbon-neutral targets by middle of this century. To implement those national pledges successfully,
accurate quantification of spatial and temporal dynamics of earth surface carbon fluxes (SCF) and closing the global carbon
budget (GCB) are essential. There are two principal approaches for SCF estimation: top-down and bottom-up. The bottom-up
40 estimates are obtained from the process-based or empirical carbon cycle models (Kondo et al., 2020; Zeng et al., 2005; Denning
et al., 1996). However, there is still a "missing" or residual carbon sink to close the GCB with bottom-up approachs because
of the limitation of our understanding of the natural carbon cycle and the lack of observations to validate the models globally.
The top-down approach optimizes the SCF by fusing the atmospheric CO_2 concentration measurements with the modeled CO_2
using the techniques such as Bayesian synthesis approach (e.g., Rodenbeck et al., 2003; Gurney et al., 2004), data assimilation
45 such as Ensemble Kalman Filters (EnKF) (e.g., Peters et al., 2005, 2007; Feng et al., 2009; Zupanski et al., 2007; Lokupitiya
et al., 2008; Bruhwiler et al., 2005) and variational methods (e.g., Baker et al., 2006; Basu et al., 2013; Chevallier et al., 2010;
Liu et al., 2014). In recent decades, the global CO_2 observation networks from surface to the air and space have provided large
amounts of high precision atmospheric CO_2 concentration data (Crevoisier et al., 2004; Crisp et al., 2017; Tans et al., 1990;
Yang et al., 2018; Yokota et al., 2009), which greatly enhance the quality of top-down estimates.

50

The CO_2 is a long-lived tracer gas, so remote observations can play an important role in estimating the local SCF. Thus, most
top-down systems do not localize the observations and set a very long assimilation window (AW) that range from several
months to one year (Chevallier et al., 2010a; Peters et al., 2007; Rodenbeck et al., 2003; Liu et al., 2014) to compromise the
sparse and unevenly distributed feature of our global CO_2 observation network. However, the atmospheric transport model
55 (ATM) generated atmosphere CO_2 will deviate from Gaussian distribution with long AW. Both EnKF and variational methods
use the linear hypothesis to constrain the system. To obtain the optimal assimilation, the forecast uncertainties are expected to
remain or close to linear. It is very hard to hold the linear perspective with a long AW. Therefore, only the SCF is considered
a valuable product, while CO_2 concentration is derived with the forward model as post-analysis.

60 Instead of treating the CO_2 as a by-product of the inversion, Kang et al. (2011, 2012) developed a top-down carbon data
assimilation system with a short AW (6 hours) to simultaneously estimate SCF and CO_2 concentration. The system includes
an online atmospheric general circulation model (AGCM) that the meteorological observations (wind, temperature, humidity,
surface pressure) and CO_2 concentration observations were assimilated simultaneously to account for the uncertainties of the
meteorological field and their impact on the transport of atmospheric CO_2. Following this effort, we have developed a LETKF-
65 based CO_2 data assimilation system (LETKF_C) to generate meaningful CO_2 analysis using a combination of a short AW (e.g.,
one day) and a long observation window (OW) (e.g., seven days) (Liu et al., 2019). The system replaces the GCM within Kang
et al. (2011, 2012) as an ATM, GEOS-Chem, to reduce the computation cost and the uncertainties of the meteorological field.

In the context of the observing system simulation experiments (OSSE), both systems (Kang et al., 2012, 2011; Liu et al., 2019) successfully reproduced the global SCF seasonal cycle and annual SCF pattern at grid-point resolution without direct SCF priori information.

A major concern for the two systems is the carbon mass conservation issue. Data assimilation (DA) systems use observations to constrain the model state statistically. The DA update process could not follow the model dynamic principle perfectly, hence, leading to a loss of mass and energy conservation and dynamic balances (Zeng et al., 2017). The impact of such imbalances could be reduced or eliminated by model dynamic adjustment in a short period, but the impact of additional mass gain or loss could last for a long time. For example, mass conservation is crucial for carbon-cycle and hydrological studies (Pan and Wood, 2006). The LETKF_C system follows the same process as the DA process to update atmospheric CO_2 directly using observation. Therefore, the carbon mass conservation will not hold within a DA cycle. To overcome this limitation, a Constrained Ensemble Kalman Filter (CEnKF) step has been applied to the newly developed Carbon of Ocean, Land, and Atmosphere data assimilation system (COLA) of version 1.0. The CEnKF was originally used in the hydrological field for data assimilation as a second constraining optimizer (Pan and Wood 2006). The basic concept for CEnKF is to constrain the global analysis mass back to the first guess. With the CEnKF added into the COLA system, we rebuild the carbon mass conservation and enhance the CO_2 and SCFs estimation.

This paper is organized as following: Section 2 briefly describes the global COLA system and CEnKF. Section 3 describes the OSSE experiments design. Section 4 present the results and analysis in the context of observing system simulation experiments (OSSE). Summary and discussion are presented in Section 5.

2   Methods

2.1 GEOS-Chem model

COLA uses GEOS-Chem as the ATM to simulate the global atmospheric CO_2 variation (Nassar et al., 2013). In this study, we use the Modern-Era Retrospective analysis for Research and Applications, Version 2 (MERRA2) (Gelaro et al., 2017) meteorology reanalysis to drive the version 13.0.2 of GEOS-Chem at $4^{\circ} \times 5^{\circ}$ horizontal resolution (native resolution of $0.5^{\circ} \times 0.625^{\circ}$) with 47 vertical levels (~30 levels below the stratosphere). The time step interval of GEOS-Chem is set as 30 minutes for both chemical process and transport.

Since the CO_2 is a passive tracer in GEOS-Chem and our assimilation system does not consider the uncertainties of metrological reanalysis, we treated different CO_2 ensemble members as different CO_2 tracers in GEOS-Chem. Therefore, we produce the ensemble simulations by running a single GEOS-Chem, instead of GEOS-Chem ensembles, which significantly saves the computational resources (acknowledgment to Dr. Fuqing Zhang for the idea, personal discussion).

100

To simulate the atmospheric CO_2 concentration evolution, GEOS-Chem is forced with the SCF, including land-atmosphere fluxes (FTA), ocean-atmosphere fluxes (FOA), and fossil fuel emissions (FFE). The total SCF at each model grid point is the parameter to be estimated in the COLA.

2.2 Four Dimensional Local Ensemble Transform Kalman Filter (4D-LETKF)

Following Liu et al. (2019), we used the four dimensional Local Ensemble Transform Kalman Filter (LETKF) as the data assimilation algorithm. The LETKF algorithm is an Ensemble Square Root Kalman Filter developed by Hunt et al. (2005, 2007). It is widely used for data assimilation, including several operational centers, and it has been applied in the joint state and parameter data assimilation problems (Ruiz et al., 2013), such as carbon data assimilations (Kang et al., 2012, 2011). Same as the other EnKF algorithms, LETKF combines background (model forecast) and observations based on their error covariance statistically to generate the analysis with reduced uncertainties. The background and analysis error uncertainty are represented by the perturbations of background $(\mathbf{x^b} = \mathbf{x_k^b} - \mathbf{\bar{x}_k^b})$ and analysis $(\mathbf{x^a} = \mathbf{x_k^a} - \mathbf{\bar{x}_k^a})$ ensembles, respectively. Where $\mathbf{x_k^b}$ and $\mathbf{\bar{x}^b}$ are the background and its mean, respectively; $\mathbf{x_k^a}$ and $\mathbf{\bar{x}^a}$ are the analysis ensemble and its mean, respectively; $\mathbf{y_k^b}$ and $\mathbf{\bar{y}^b}$ are the forecast observations and their mean, respectively. The $\mathbf{y_k^b} = \mathbf{H}(\mathbf{x_k^b})$ projects the background from the model space to the observation space with the observation operator $\mathbf{H}$. The overall LETKF algorithm is summarized as follows,

$$\mathbf{\bar{x}^a} = \mathbf{\bar{x}^b} + \mathbf{X^b}\mathbf{\bar{w}} \tag{1}$$

$$\mathbf{\bar{w}} = \mathbf{\widetilde{P}^a}\left(\mathbf{Y^b}\right)^{\mathbf{T}}\mathbf{R^{-1}}\left(\mathbf{y^o} - \mathbf{\bar{y}^b}\right) \tag{2}$$

$$\mathbf{\widetilde{P}^a} = [\left(\mathbf{Y^b}\right)^{\mathbf{T}}\mathbf{R^{-1}}\left(\mathbf{Y^b}\right) + (K-1)\mathbf{I}]^{-1} \tag{3}$$

$$\mathbf{X^a} = \mathbf{X^b}[(K-1)\mathbf{\widetilde{P}^a}]^{\frac{1}{2}} \tag{4}$$

Here $\mathbf{X^b}\mathbf{\bar{w}}$ is the analysis increment applied to each ensemble member, with $\mathbf{R}$ denoting the observation error covariance, $\mathbf{\widetilde{P}^a}$ is the analysis error covariance, K is the number of ensemble members, $\mathbf{I}$ is the identity matrix. LETKF simultaneously assimilates all observations within a certain distance at each model grid point, which defines the localization scale. Hunt et al. (2005) introduced a four-dimensional version, and (Hunt et al., 2007) provided detailed documentation of the 4-D LETKF that we are using in this study.

125

Previous work has shown that the LETKF can be successfully applied to estimate SCFs and CO_2 concentration simultaneously using atmospheric CO_2 observations (Kang et al., 2012, 2011; Liu et al., 2012; Liu et al., 2019). The SCFs are treated as parameters augmenting to the state vector C (the prognostic variable of atmospheric CO_2), $\mathbf{X} = [\mathbf{C}, \mathbf{SCF}]^{\mathbf{T}}$. An EnKF usually assumes the estimated parameters as special variables that are stationary during model integration. Therefore, the first guess of the parameter is the persistence of their analysis from the last analysis cycle. Though the SCF evolves with time, the

parameter estimation can still produce decent estimation if the SCF is slowly evolving and the AW is short enough (Ruiz et al., 2013). We set the AW to 1 day, while a run-in-place method is applied (Kalnay and Yang, 2010) by setting an additional observation window (OW) of 6 days. The estimation also benefits from more observations. The overall window (OAW) is one week.

2.3 Constrained Ensemble Kalman Filter (CEnKF)

As previously discussed, the LETKF and most of the ensemble-based Kalman Filter do not maintain the physic bound of the state and conservation of physical laws of state dynamic (Zeng et al., 2017). Since the LETKF process destroys the carbon mass conservation (Fig. 1), we applied a Constrained Ensemble Kalman Filter (CEnKF) to constrain the global mass of state $\mathbf{C}$ after the LETKF process. The concept was based on Pan and Wood (2006) that applied the CEnKF to balance the water budget for each ensemble member. We further simplified the method by constraining only the ensemble mean state, which significantly reduced the computational cost without influencing the performance.

The mass conservation is destroyed by adding or reducing mass during DA updating. We can rebuild the mass conservation by moving the mass back to their original values (before the DA update). Our target is to retain the global mass conservation,

$$\mathbf{M^a} - \mathbf{M^b} = \mathbf{0} \tag{5}$$

Where $\mathbf{M^a}$ and $\mathbf{M^b}$ are the expected analysis and the first guess global CO_2 mass, respectively. The transformation from CO_2 concentration at each grid to a global CO_2 mass could be expressed as,

$$\mathbf{M} = \mathbf{H\bar{C}} \tag{6}$$

Where $\mathbf{H}$ is the linear "observation" operator that transforms the global 3D CO_2 concentration to the global CO_2 mass. At each grid, the operator is proportional to the air mass. Now the question becomes how to distribute the expected global total mass adjustment to each model grid point. CEnKF achieves this by applying an EnKF steps with the $\mathbf{M^b}$ as "observations" and takes the constraint as the "observation" equation. We add the constraint to the common EnKF formula as,

$$\mathbf{\bar{C}^{a+}} = \mathbf{\bar{C}^a} + \mathbf{E^a}(\mathbf{HE^a})^\mathbf{T}(\mathbf{HE^a}(\mathbf{HE^a})^\mathbf{T} + \mathbf{R})^{-1}(\mathbf{H\bar{C}^b} - \mathbf{H\bar{C}^a}) \tag{7}$$

Where $\mathbf{\bar{C}^{a+}}$ is the CEnKF CO_2 ensemble mean. $\mathbf{\bar{C}^a}$ is the LETKF ensemble mean of CO_2. $\mathbf{E^a}$ is ensemble perturbation of CO_2 after the LETKF process. CEnKF defines the "observations" as the truth with $\mathbf{R} = \mathbf{0}$ to meet the mass conservation purpose. Therefore, the EnKF equation is written as,

$$\mathbf{\bar{C}^{a+}} = \mathbf{\bar{C}^a} + \mathbf{E^a}(\mathbf{HE^a})^\mathbf{T}(\mathbf{HE^a}(\mathbf{HE^a})^\mathbf{T})^{-1}(\mathbf{H\bar{C}^b} - \mathbf{H\bar{C}^a}) \tag{8}$$

which is the original EnKF algorithm (Evensen, 1994). The perturbed observation step is not needed with $\mathbf{R} = \mathbf{0}$. Note we are not using LETKF here because it cannot handle the condition of $\mathbf{R} = \mathbf{0}$ (Eq. 3). Generally, CEnKF distributes the global mass adjustment to each grid point by taking advantage of the ensemble perturbation $\mathbf{E^a}$ given by the LETKF. The grid with a larger ensemble spread will likely give more mass constraints.
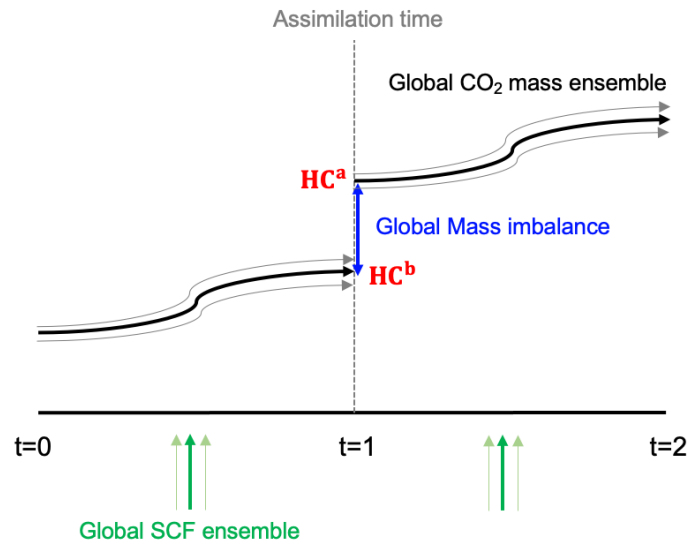
Figure 1: Schematic illustration of the mass imbalance problem.

165

2.4 Inflation

Inflation and localization are the commonly used techniques to improve the filter performance for EnKF applications. The ensemble is expected to underestimate the forecast uncertainties because of the error sources such as limited ensemble size and model deficiencies. The negative ensemble variance can degrade the filter performance, and in severe cases, lead to filter

170 divergence where the filter will reject the observations. Inflation plays an important role to compensate the negative ensemble variance, which can be separated into three categories: multiplicative inflation, relaxation inflation, and additive inflation (Anderson, 2007; Mitchell and Houtekamer, 2000; Zhang et al., 2004; Whitaker et al., 2008; Whitaker and Hamill, 2012; Miyoshi, 2011). We update our inflation strategy from Liu et al. (2019) to better fit the mass conservation requirement. The original additive inflation for CO_2 in Liu et al. (2019) does not preserve the carbon mass conservation in the atmosphere.

175 Therefore, for CO_2, we apply the relaxation to prior spread (RTPS) scheme from Whitaker and Hamill (2012), which combined the relaxation to prior perturbation (RTPP) logic from Zhang et al. (2004) into the multiplicative inflation approach,

$$\mathbf{C_k^a} = \overline{\mathbf{C^a}} + \boldsymbol{\gamma} \cdot (\mathbf{C_k^a} - \overline{\mathbf{C^a}}) \tag{9}$$

$$\boldsymbol{\gamma} = \mathbf{1} + \boldsymbol{\alpha} \cdot \frac{\sigma^b - \sigma^a}{\sigma^a} \tag{10}$$

Where $\boldsymbol{\sigma}$ is the ensemble spread, α is the scaling factor. In this study, we set α to 0.7.

180

We retained the additive inflation for the SCFs as in Liu et al. (2019) with a slight adjustment. We treat the SCFs as the parameter for estimation in our system. However, the SCFs are the boundary forcing with temporal evolution that is missing in our dynamic model. The additive inflation scheme was designed to add the missing uncertainties into the system. It prevents the effective ensemble dimension from collapsing toward the dominant directions of error growth (Whitaker et al.,

185 2008). Since we do not know about the SCF uncertainty globally and at each grid, we use the priori SCF annual cycle as the benchmark. For FTA, the added perturbation fields are selected randomly from the SiB3 (Denning et al., 1996). After each LETKF process, the ensemble spread at each point is inflated back to the predefined uncertainty by additively adding random fields selected from prior SCF within one year centered at assimilation time (Kang et al., 2012; Liu et al., 2019). Instead of randomly perturbing the ensembles based on a distance-decaying model (Wu et al., 2013), the additive inflation takes

190 advantage of the prior randomness,

$$\mathbf{SCF_k^a} = \mathbf{SCF_k^a} + \mathbf{\Gamma} \cdot \left(\mathbf{SCF_k^{ps}} - \overline{\mathbf{SCF^{ps}}} \right) \tag{11}$$

Where the subscript **k** denotes the **k**th ensemble member, the superscript **ps** denotes the sampled prior SCF. **Γ** is the factor that rescales the sample spread to the predefined magnitude. We retain the same localization scheme and ensemble size of 20 as in Liu et al. (2019).

3   Design of the Observing System Simulation Experiment (OSSE)

3.1 Prescribed fluxes and initial conditions

The experiments span from 1 October 2014 to 1 January 2018. In this paper, we only focused on the FTA. The FFE and FOA are treated as background fluxes that are the same in the prior SCF and true SCF. The FFE is the hourly Open-source Data Inventory of Anthropogenic CO_2 emission (ODIAC) (Oda and Maksyutov, 2011). It was disaggregated from monthly to hourly

200 based on the TIMES method (Nassar et al., 2013). We use a monthly pCO_2 interpolated FOA product (Gruber et al., 2019). We use the daily FTA simulated by the VEGAS model (Zeng et al., 2005) as true FTA. In contrast, we used the daily FTA modeled by SiB3 in the year 2008 as priori for all of the years (Denning et al., 1996). Moreover, the priori annual mean is subtracted. Thus, there is no inter-annual variation and mean source-sink information coming from the priori FTA. As mentioned in Sec. 2.4, the priori FTA are used to inflate the FTA ensembles.

205

The initial CO_2 condition of the nature run for 1 October 2014 is generated forcing by the true SCF run from 1 January 2014. To get the prior ensemble initial CO_2 and SCF condition, we established a control run starting from 1 January 2014 using prior SCF, then randomly selected from the control run center at 1 October 2014 within 30 days. The ensemble mean initial SCF and CO_2 conditions are significantly larger than the truth over the northern forest region (Fig. 7). Thus, spin-up is always

210 needed in this OSSE or real-world scenario to reach a near unbiased state. We spin up the system from 1 October 2014 to 1 January 2015 to get a jointly stable CO_2 state and SCF parameter.

3.2 Pseudo observations

The specific time, location, and observation error of the actual data are used to generate the pseudo observations. The CO_2

215 GLOBALVIEWplus v6.0 ObsPack is the primary source of surface data (Schuldt et al., 2020). Since there are few stations

over Siberia, we included several tower observations obtained by the National Institute for Environmental Studies (NIES) (Sasakawa et al., 2010). For satellite data, we used Orbiting Carbon Observatory-2 (OCO-2) data (Crisp et al., 2017). Since we are focusing on the CEnKF impact, we considered only the experiments that are based on both surface and OCO-2 observations, and the influence of the two different observation networks is not considered. We plan to address the potential

220 effects of such differences in future studies.

The observation error is an essential part of the assimilation. Generally, the error is the sum of instrument error (R_I) and representative error (R_R). For the surface observations, to estimate R_R at each site, we followed Chevallier et al. (2010a) that used the standard deviation of the detrended and deseasonalized data as a proxy. Overall, the error ranged from less than 0.1

225 ppm at the south pole (SPO) to over 10 ppm at some tower stations (Fig. 2).

The original OCO-2 sampling pixel is relatively small (~3km) compared with the model grid size. Moreover, there are around four hundred soundings along every latitude. Thus, appropriate data thinning and filtering are necessary. In addition, the retrieval error needs to be estimated. We used a post-processed OCO-2 level 2 data based on a new exponentially-decaying

230 error correlation model with a length scale computed from airborne lidar measurements (Baker et al., 2021). Since ocean glint observations have system bias compared with land observations (Crowell et al., 2019), only the land nadir and land glint data are assimilated (Fig. 3).
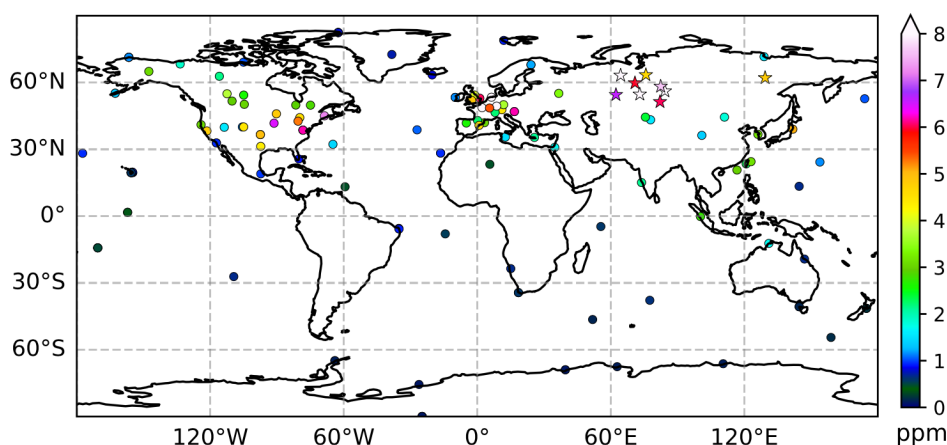
235 **Figure 2: The location of the pseudo surface observations. The dots are the GLOBALVIEW-CO2 observations, and the pentagram is the AMES tower observations. The different colors represent the representative error of each station.**
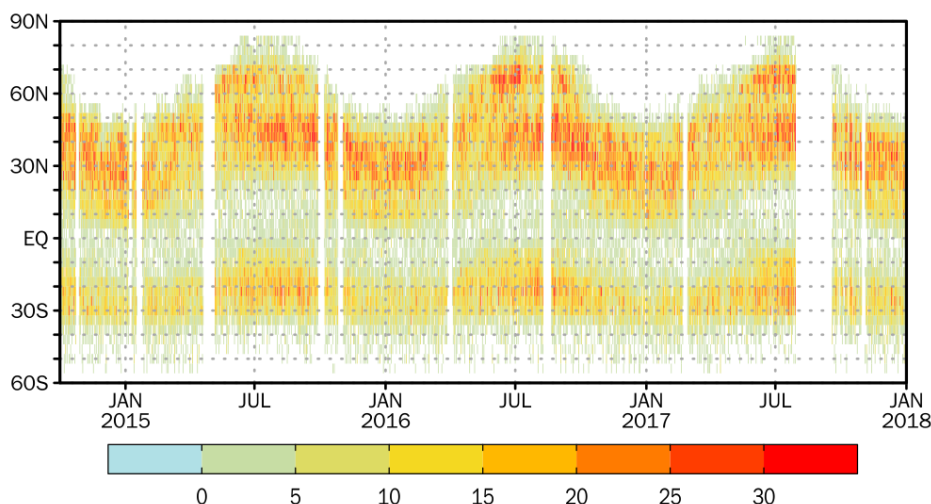
Figure 3: The daily pseudo OCO-2 land-nadir and land-glint retrievals numbers along the latitudes.

3   OSSE results

In this section, we present the seasonal cycle (SC) and inter-annual variation (IAV) of FTA estimated by the improved COLA system. Then we systematically investigate the impact of CEnKF on the estimation of FTA and CO_2 on the annual scale by comparing with an experiment without CEnKF (Table. 1).

Table 1: Summary of the experiment setup. We conducted two different experiments using different assimilation schemes of LETKF (L) and LETKF together with CEnKF (LC). There is no inter-annual variation (IAV) and annual mean source and sink (AMSS) information in the prior.

	EXP-LC	EXP-L
DA Scheme	LETKF+CEnKF	LETKF only
AW+OW	1+6 days	
Ensemble Member	20	
Prior FTA	SiB3 (without IAV and AMSS)	
True FTA	VEGAS	

4.1   Seasonal cycle and inter-annual variation

First, we show the performance of the improved COLA system at the seasonal scale. Globally, the larger SC amplitude of the priori is corrected, and the SC phase is fixed too (Fig. 4a). The global or regional analysis root-mean-square error (RMSE) for FTA is calculated as follows,

$$\text{RMSE}_{\text{reg}}^{\text{a}} = \sqrt{E_t((\text{SCF}^{\text{a}}(t, \text{reg}) - \text{SCF}^{\text{t}}(t, \text{reg}))^2)} \tag{12}$$

255 and the priori FTA $\text{RMSE}_{\text{reg}}^{\text{p}}$ can be calculated using the same fomula. We further define the RMSE reduction from priori to analysis,

$$\text{RMSER}_{\text{reg}}^{\text{a}} = \frac{\text{RMSE}_{\text{reg}}^{\text{p}} - \text{RMSE}_{\text{reg}}^{\text{a}}}{\text{RMSE}_{\text{reg}}^{\text{p}}} \tag{13}$$

The RMSER of the global daily FTA is 28% (Fig. 4b). While zooming into the continental regions monthly, the RMSE over all these regions significantly decreases (Fig. 5, 6). This reduction ranges from 43% to 90%. Over the North extratropical
260 region, where there are dense observations, the reduction exceeds 71%. The most significant error reduction occurs over the Eurasia boreal region.

Over the tropical and southern extratropical region, the RMSER is smaller. Since there are fewer observations, the accurate estimation over those regions is more challenging. However, the SC amplitude and phase are reinvestigated except for Northern
265 Africa (NAF) and Southern Tropical South America (STSA). Over NAF, the FTA is close to the prior FTA during the growing season. Over STSA, the SC phase shows a one-month lag, while the SC amplitude is fixed.

Since the OSSE period covers the 2015-2016 El Nino event, the tropical FTA of the truth shows a large IAV. In contrast, the IAV is smaller over the northern hemisphere. The EXP-LC showed that the IAV is well reproduced without leaking from
270 tropical to the northern hemisphere (Fig. 5, 6). However, the IAV may leak between adjacent OCO2MIP regions (Crowell et al., 2019). The IAV is larger than truth over Eurasia Boreal and smaller than truth over Europe from January 2017 to Jun 2017. A similar phenomenon also occurs over the North American continent and South American continent. Since there is no IAV in the priori FTA, we hypothesis that the IAV estimation could be improved using prior FTA with IAV.

275 Focusing on the grided scale, the bias of EXP-LC compared with priori is significantly reduced during all the seasons (Fig. 7). The largest difference of the priori compared with truth occurred over the Northern hemisphere forest region, where the seasonal cycle amplitude is large. A significant bias can also be seen from the regional total time series (Fig. 5). Over the tropical region, the priori is also significantly biased, especially for Tropical South America and Northern Africa. By contrast, the bias of EXP-LC is much smaller and evenly distributed. In addition, its bias is relatively larger during summer than in the
280 other seasons.
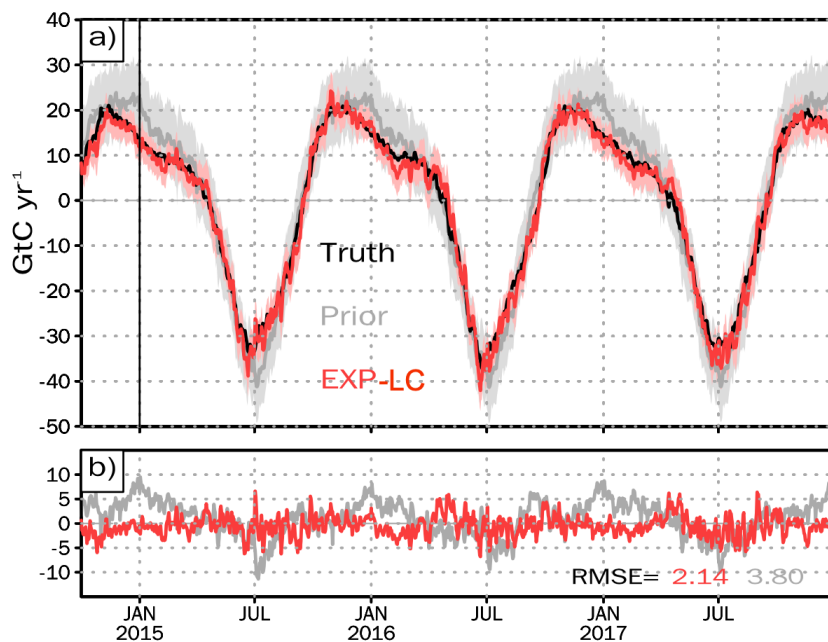
Figure 4: a) The global daily FTA of truth (black), prior (grey), and analysis of EXP-LC (red). The vertical line on 1 January 2015 indicates the start of assimilation. Before 1 January 2015, the system spin-up for three months. b) The difference compared with the truth.

285
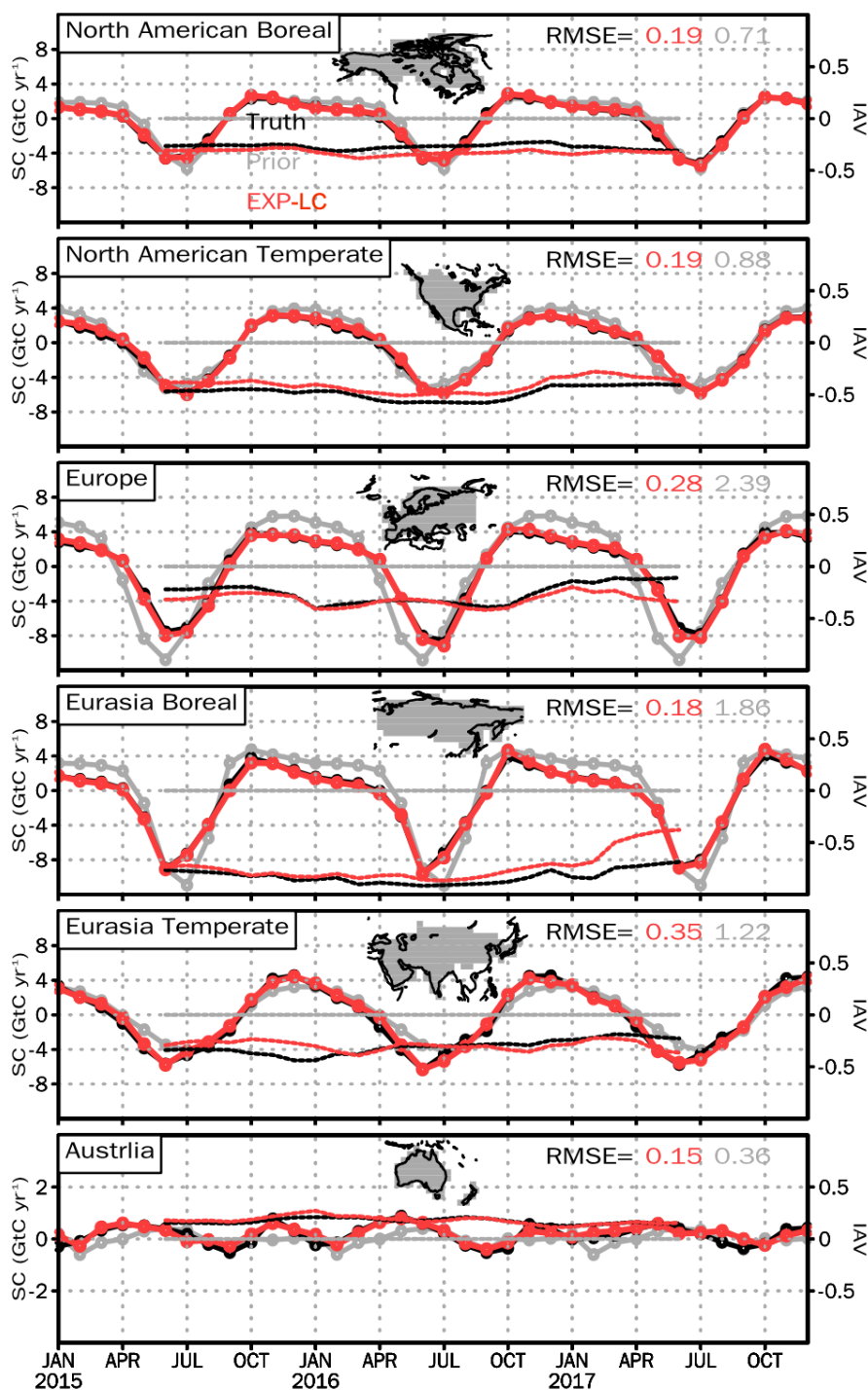
Figure 5: The FTA seasonal cycle (SC) and inter-annual variation (IAV) over the northern hemisphere regions and Australia given by truth (black), prior (grey), and estimated from EXP-LC (red). The solid lines with open circles marked on them are the SC. The dash lines are the IAV calculated using a 12-month temporal smoother that the seasonal cycle is filtered out.

290
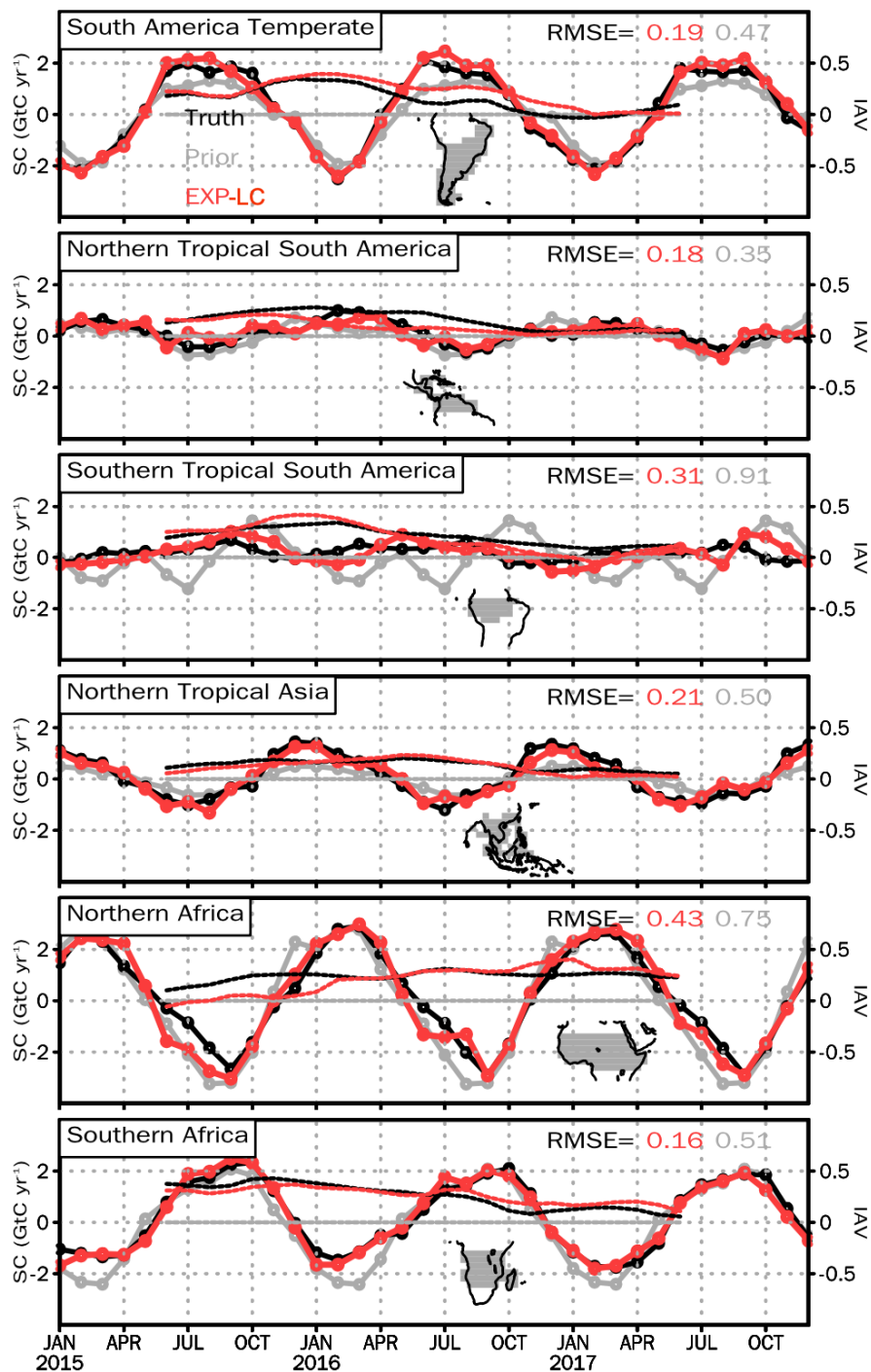
Figure 6: Same as Figure 5, but for the tropical regions.

295
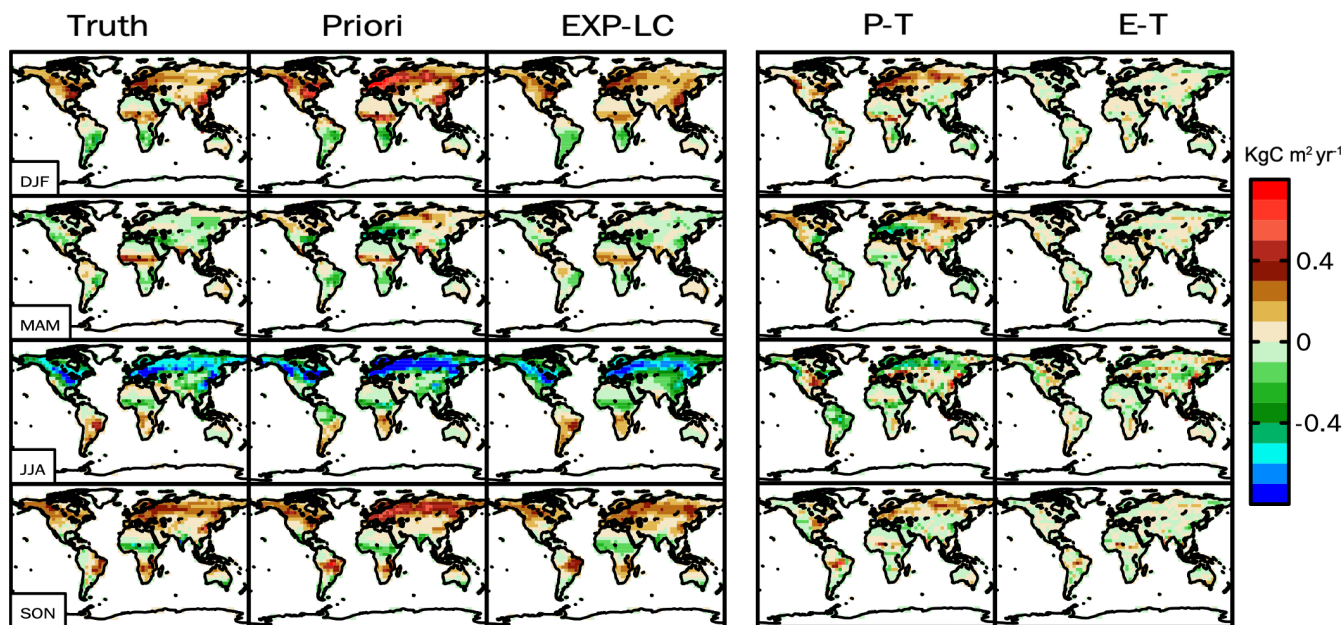
Figure 7: The left three columns are the climatological seasonal cycle of the truth, priori, and EXP-LC from December to February (DJF), March to May (MAM), June to August (JJA), and September to November (SON). The right two columns are the difference between the priori and truth (P-T) and between the EXP-LC and truth (E-T).

300

4.2 The Impact of CEnKF on Annual Flux Estimation

In the above section, we showed the performance of the COLA system at the seasonal scale. The improvement of CEnKF manifested while zooming into the annual scale. To illustrate its impact, we conduct a contrast experiment without CEnKF (EXP-L). For EXP-L, the acculation of the annual global imbalances is 0.154, 0.173, and 0.024 GtC for 2015, 2016, and

305 2017 (Fig. 8). Such imbalance is not negligible compared with the annual mean FTA of around -1.2 GtC. Moreover, the bias compared with truth is -0.191, -0.267, and -0.024 GtC for 2015, 2016, and 2017. For EXP-LC without mass imbalance issue, the annual FTA estimation is improved with less than 0.06 GtC bias for all the years (Fig. 8). The significantly reduced bias indicates that CEnKF could efficiently help the global flux estimation.

310 Regionally, the performance of EXP-LC is also better than EXP-L over most of the OCO2MIP regions (Crowell et al., 2019) except Europe, Eurasia boreal, and South America temperate (Fig. 9). Over the Eurasia temperate, Australia, Southern Tropical South America, and Southern Tropical Africa, EXP-LC is almost the same as the truth. For both EXP-LC and EXP-L, the source or sink is well consistent with the truth. However, the FTA is reversed from a source to a small sink in Northern Tropical Asia for EXP-L.

315
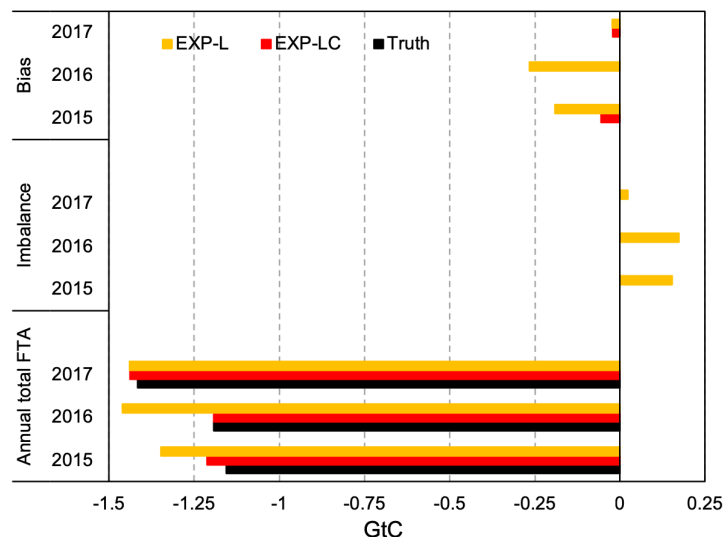
Figure 8: The global annual total FTA, imbalance, and Bias of EXP-LC (LETKF+CEnKF) and EXP-L (LETKF) compared with truth in 2015, 2016, and 2017. Note that there is no imbalance problem for EXP-LC that there are no imbalance bars.

320
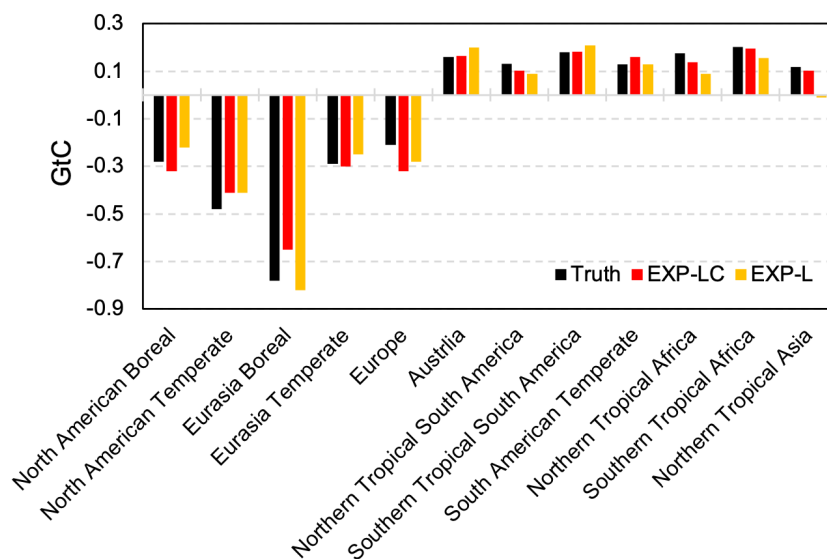
Figure 9: The total regional FTA of EXP-LC and EXP-L compared with truth from January 2015 to December 2017. Fig. 5 and Fig. 6 draw the OCO2MIP region.
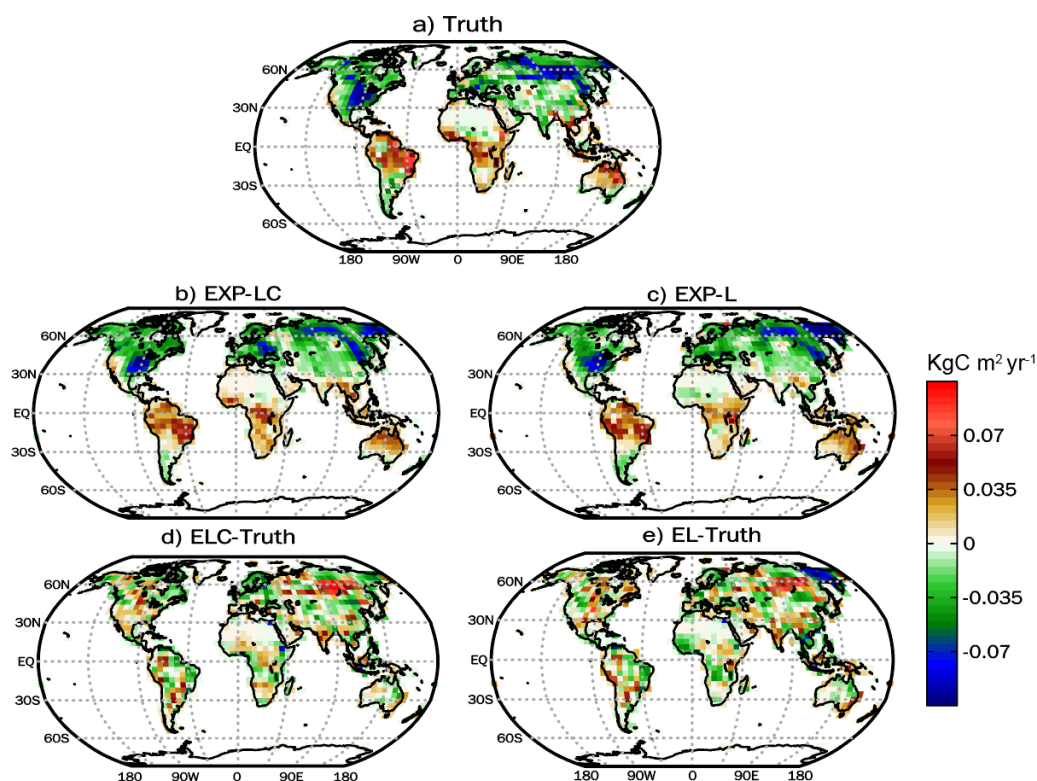
325

Figure 10: The spatial distribution of FTA for truth (a), EXP-LC (b), EXP-L (c) averaged from January 2015 to December 2017. The annual mean of the prior FTA is not shown because it is zero at each grid. The bias of EXP-LC (ELC) compared with truth (d) and EXP-L (EL) compared with truth (e).

330   For both EXP-LC and EXP-L, the FTA pattern is well reproduced at the grid-scale (Fig. 10b, c). The widespread carbon sink over the Northern hemisphere and carbon source over the tropical and southern hemisphere are reproduced. Furthermore, the carbon source over the Southern China and the carbon sink over Southern South America are reinvestigated. However, EXP-L shows slightly better results than EXP2 (Fig. 10c). Over North America, EXP-LC shows a clearer west-east dipole pattern compared with EXP-L. Over northern tropical Africa, EXP-LC successfully estimates the carbon source at the side and carbon

335   sink at the center. Even though the FTA pattern difference between EXP-LC and EXP-L is not significant, the improved fine-scale FTA estimation indicates that the CEnKF may improve the global to regional carbon budget estimation and improve the grided estimation at the annual scale. For both experiments, the carbon sink over Central Russia is shifted northward (Fig 10d, e).

340   **4.3   The Impact of CEnKF on the CO_2 Estimation**

Since the CEnKF is applied to the state CO_2, we further analyze the impact of CEnKF on the state CO_2 from the DA increment

perspective (Fig. 11). After the LETKF process, the CO_2 tracers are redistributed horizontally (Fig. 11a, d) and vertically. Then, the CEnKF process conducts another redistribution that counterbalances the superfluous LETKF increment (Fig. 11b, e). Horizontally, the increment of both LETKF and CEnKF is larger over the land region. The spatial pattern of LETKF increment

345 and CEnKF increment are opposite in most regions. However, the magnitude of CEnKF increment is much smaller than LETKF, which indirectly suggests that the CEnKF assists in improving the assimilation results without overriding the LETKF increment. Finally, the global mass of the overall increment is zero, further confirming the benefits of CEnKF in overcoming the limitation of LETKF in constraining mass.
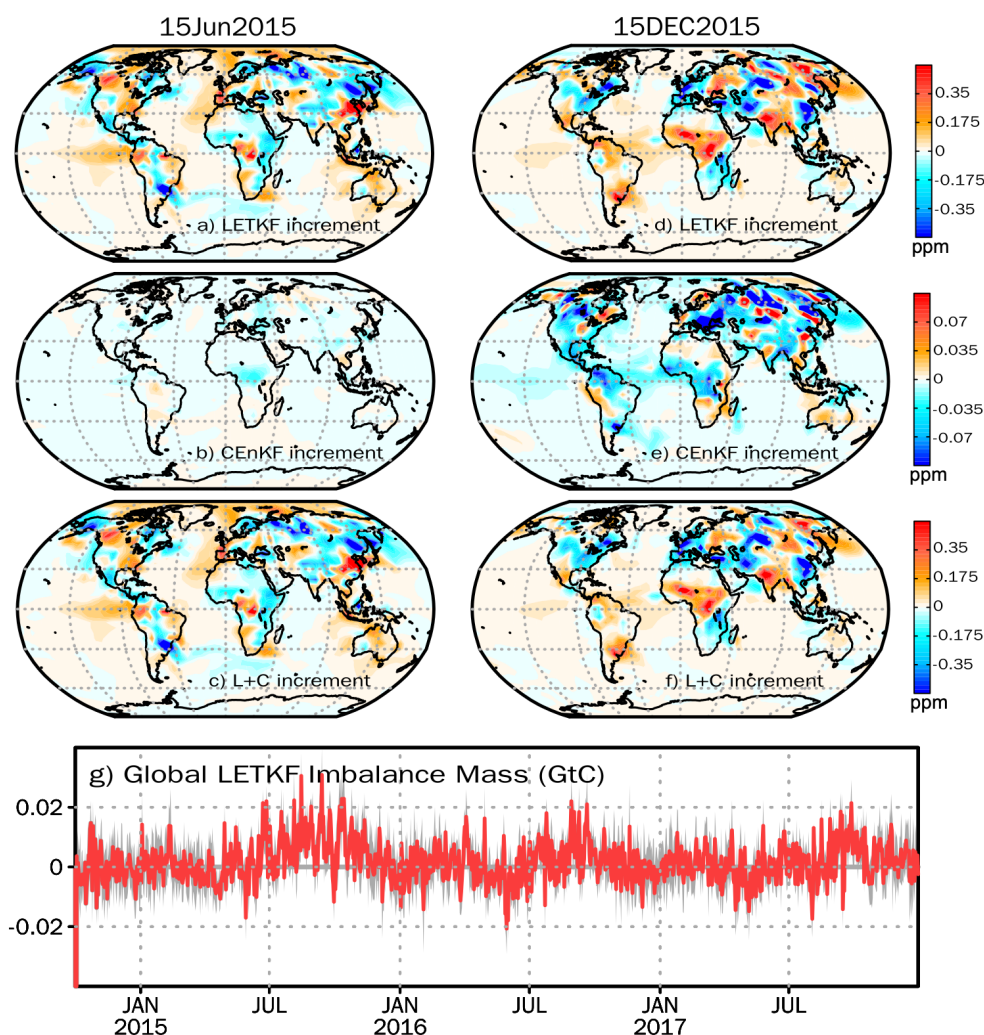
350

Figure 11: The ensemble mean LETKF and CEnKF increment of the surface CO_2 at 15 June 2015 (a~c) and 15 December 2015 (d~f) for EXP-LC. (g) The global mass imbalance caused by LETKF. The red line is the ensemble mean of the global mass imbalance. The grey shading indicates the ensemble imbalance spread.

355 The time series of the global imbalance shows that it is less than 0.03 GtC at every assimilation time (Fig. 11g). The imbalance is smaller from September to May than the rest of the months, and there is no significant positive or negative bias. From June to August, the imbalance is usually positive and more significant than the other months/seasons. At the start of the spin-up period, the imbalance is out of the image range. Because of the significantly biased initial CO_2 and FTA condition, the CO_2 state is not consistent with the SCF, which leads to the large imbalance. The additional CEnKF process helps the LETKF

360 without accumulating the error, and appears to be a reasonable approach to counterbalance the imbalance between state CO_2 and parameter SCF.

5   Summary and Discussion

In this study, we described the development of the COLA system using the CEnKF and improved inflation scheme. The COLA

365 system shows improved performance in a variety of OSSEs to assess the spatial and temporal variability of SCFs and CO_2.

By assimilating the pseudo surface and OCO-2 observations, LETKF could efficiently estimate the spatial pattern of the annual mean sources and sinks. However, without mass conservation, the annual global FTA is significantly biased. After the CEnKF process, the CO_2 mass is constrained without disruption but improving the LETKF estimation. Moreover, the constrained CO_2

370 state helps improve the estimation of annual FTA from global to regional scale. On the seasonal scale, the improved system shows compelling results. The biased seasonal cycle amplitude and phase from the priori are corrected over most of the continental regions. The estimation is relatively better over the Northern hemisphere, where the observations are dense as compared with the other regions with a smaller number of observations.

375 Because of the sparse observation network over tropical regions, most inversion systems use a very long OAW to track the tropical fluxes from the remote observations. However, the performance of COLA over the tropical region is also compelling. Using a short AW of one day, the problem of lacking a dynamic SCF model is alleviated as the ensembles could be evolved as linearly as possible and remain gaussian. Moreover, the persistent forecast model is reasonable using an AW as short as possible. Instead of abandoning the error transport property of EnKF and using prior SCF as the first guess in each AW, the SCF

380 ensembles could be transported between AWs, indicating that LETKF could learn from the previous AWs and give a more precise first guess for the current AW without iteration. The future observations in the OW and the ensembles transport from previous AW significantly reduce the dependency of very long OAW. As most inversion systems do not update the CO_2 state, one of the advantages of updating the CO_2 state is that the system does not need perfect initial conditions at the start of assimilation. After one to three months of free spin-up, the system could create jointly stable initial CO_2 and SCF conditions.

385 In addition, the update of CO_2 at each assimilation cycle could reduce the error from the previous AWs and make the signal of

the current SCF clearer and more sensitive. In conclusion, the COLA system does not need a very long OAW.

As mentioned in Sect. 2.4, 20 ensemble members could give accurate SCF estimation in the COLA system. In comparison, most ensemble-based ACI systems use ensemble members larger than 100 based on the geographic division (Feng et al., 2009;
390 Peters et al., 2007). The underlying reason is that the COLA system perturbs the ensembles using additive inflation based on the priori SCF, which introduces the priori randomness. Thus, there are physical correlations between each grid. While perturbing the ensembles based on the distance-decaying model is a widely used statistical method, the choice of the decaying length is usually subjective. Moreover, the small ensemble members significantly reduce the computer time. For example, the computer time required in the OSSE is about one and half minutes per assimilation cycle using 20 cores of Intel Xeon E5-
395 2650. Thus, the three years of OSSE only used less than one and half days of computer time.

The transport model error is always a big issue in the ACI studies. Several model inter-comparison projects have found that the transport model uncertainty is at the same order of SCF uncertainty (Baker et al., 2006a; Basu et al., 2018; Crowell et al., 2019; Schuh et al., 2019; Chevallier et al., 2010b). Therefore, quantitative transport uncertainty estimation is needed to obtain
400 a robust estimate of SCF and provide information to policymakers. The EnKF can efficiently online estimate the transport uncertainty by perturbing the meteorology state (Kang et al., 2011; Liu et al., 2011; Chen et al., 2019). At the same time, the estimation of transport uncertainty needs to update the CO_2 state and meteorology state together, which will inevitably cause the mass imbalance problem. The CEnKF method proposed here overcomes this limitation and offers a computationally efficient way of constraining the global mass.

405 *Code and data availability.* The related code for GEOS-Chem and LETKF can be accessed from http://wiki.seas.harvard.edu/geos-chem (last access: 18 March 2021; GEOS-Chem, 2021) and https://github.com/takemasa-miyoshi/letkf (last access: 18 June 2019; Miyoshi, 2019), respectively.

Author contributions. ZL conceived the CEnKF scheme. ZL, NZ, YL, and EK developed this system. QC supply the VEGAS model output. ZL designed and ran the experiments. ZL, NZ, and YL wrote the paper. All contributed to the preparation of this
410 paper.

Acknowledgments. Thanks to Zhimin Zhang for his contribution to develop the computer environment.

Financial support. This work was supported by the National Key R&D Program of China (No. 2017YFB0504000).

Reference

Anderson, J. L.: An adaptive covariance inflation error correction algorithm for ensemble filters, Tellus Dyn. Meteorol.
415   Oceanogr., 59, 210–224, https://doi.org/10.1111/j.1600-0870.2006.00216.x, 2007.

Baker, D. F., Law, R. M., Gurney, K. R., Rayner, P., Peylin, P., Denning, A. S., Bousquet, P., Bruhwiler, L., Chen, Y.-H.,
Ciais, P., Fung, I. Y., Heimann, M., John, J., Maki, T., Maksyutov, S., Masarie, K., Prather, M., Pak, B., Taguchi, S., and
Zhu, Z.: TransCom 3 inversion intercomparison: Impact of transport model errors on the interannual variability of regional
CO_2 fluxes, 1988-2003, Glob. Biogeochem. Cycles, 20, https://doi.org/10.1029/2004GB002439, 2006a.

420   Baker, D. F., Doney, S. C., and Schimel, D. S.: Variational data assimilation for atmospheric CO_2, Tellus B Chem. Phys.
Meteorol., 58, 359–365, https://doi.org/10.1111/j.1600-0889.2006.00218.x, 2006b.

Baker, D. F., Bell, E., Davis, K. J., Campbell, J. F., Lin, B., and Dobler, J.: A new exponentially-decaying error correlation
model for assimilating OCO-2 column-average CO2 data, using a length scale computed from airborne lidar measurements,
Geosci Model Dev Discuss, 29, https://doi.org/10.5194/gmd-2020-444, 2021.

425   Basu, S., Guerlet, S., Butz, A., Houweling, S., Hasekamp, O., Aben, I., Krummel, P., Steele, P., Langenfelds, R., Torn, M.,
Biraud, S., Stephens, B., Andrews, A., and Worthy, D.: Global CO_2 fluxes estimated from GOSAT retrievals of total column
CO_2, Atmospheric Chem. Phys., 13, 8695–8717, https://doi.org/10.5194/acp-13-8695-2013, 2013.

Basu, S., Baker, D. F., Chevallier, F., Patra, P. K., Liu, J., and Miller, J. B.: The impact of transport model differences on CO_2
surface flux estimates from OCO-2 retrievals of column average CO_2, Atmospheric Chem. Phys., 18, 7189–7215,
430   https://doi.org/10.5194/acp-18-7189-2018, 2018.

Bruhwiler, L. M. P., Michalak, A. M., Peters, W., Baker, D. F., and Tans, P.: An improved Kalman Smoother for atmospheric
inversions, Atmospheric Chem. Phys., 5, 2691–2702, 2005.

Chen, H. W., Zhang, F., Lauvaux, T., Davis, K. J., Feng, S., Butler, M. P., and Alley, R. B.: Characterization of Regional-
Scale CO_2 Transport Uncertainties in an Ensemble with Flow-Dependent Transport Errors, Geophys. Res. Lett., 46, 4049–
435   4058, https://doi.org/10.1029/2018GL081341, 2019.

Chevallier, F., Ciais, P., Conway, T. J., Aalto, T., Anderson, B. E., Bousquet, P., Brunke, E. G., Ciattaglia, L., Esaki, Y.,
Fröhlich, M., Gomez, A., Gomez-Pelaez, A. J., Haszpra, L., Krummel, P. B., Langenfelds, R. L., Leuenberger, M., Machida,
T., Maignan, F., Matsueda, H., Morguí, J. A., Mukai, H., Nakazawa, T., Peylin, P., Ramonet, M., Rivier, L., Sawa, Y.,
Schmidt, M., Steele, L. P., Vay, S. A., Vermeulen, A. T., Wofsy, S., and Worthy, D.: CO_2 surface fluxes at grid point scale
440   estimated from a global 21 year reanalysis of atmospheric measurements, J. Geophys. Res., 115, D21307,
https://doi.org/10.1029/2010JD013887, 2010a.

Chevallier, F., Feng, L., Bösch, H., Palmer, P. I., and Rayner, P. J.: On the impact of transport model errors for the estimation
of CO2 surface fluxes from GOSAT observations, Geophys. Res. Lett., 37, L21803,
https://doi.org/doi:10.1029/2010GL044652, 2010b.

445   Crevoisier, C., Heilliette, S., Chédin, A., Serrar, S., Armante, R., and Scott, N. A.: Midtropospheric CO_2 concentration retrieval

from AIRS observations in the tropics, Geophys. Res. Lett., 31, L17106, https://doi.org/10.1029/2004GL020141, 2004.

Crisp, D., Pollock, H. R., Rosenberg, R., Chapsky, L., Lee, R. A. M., Oyafuso, F. A., Frankenberg, C., O'Dell, C. W., Bruegge, C. J., Doran, G. B., Eldering, A., Fisher, B. M., Fu, D., Gunson, M. R., Mandrake, L., Osterman, G. B., Schwandner, F. M., Sun, K., Taylor, T. E., Wennberg, P. O., and Wunch, D.: The on-orbit performance of the Orbiting Carbon Observatory-2
450   (OCO-2) instrument and its radiometrically calibrated products, Atmospheric Meas. Tech., 10, 59–81, https://doi.org/10.5194/amt-10-59-2017, 2017.

Crowell, S., Baker, D., Schuh, A., Basu, S., Jacobson, A. R., Chevallier, F., Liu, J., Deng, F., Feng, L., McKain, K., Chatterjee, A., Miller, J. B., Stephens, B. B., Eldering, A., Crisp, D., Schimel, D., Nassar, R., O'Dell, C. W., Oda, T., Sweeney, C., Palmer, P. I., and Jones, D. B. A.: The 2015–2016 carbon cycle as seen from OCO-2 and the global in situ network,
455   Atmospheric Chem. Phys., 19, 9797–9831, https://doi.org/10.5194/acp-19-9797-2019, 2019.

Denning, A. S., Randall, D. A., Collatz, G. J., and Sellers, P. J.: Simulations of terrestrial carbon metabolism and atmospheric CO2 in a general circulation model. Part 2: Simulated CO2 concentrations, Tellus B, 48, 543–567, https://doi.org/10.1034/j.1600-0889.1996.t01-1-00010.x, 1996.

Evensen, G.: Sequential data assimilation with a nonlinear quasi-geostrophic model using Monte Carlo methods to forecast
460   error statistics, J. Geophys. Res., 99, 10143, https://doi.org/10.1029/94JC00572, 1994.

Feng, L., Palmer, P. I., Bosch, H., and Dance, S.: Estimating surface CO2 fluxes from space-borne CO2 dry air mole fraction observations using an ensemble Kalman Filter, Atmospheric Chem. Phys., 9, 2619–2633, 2009.

Friedlingstein, P., Cox, P., Betts, R., Bopp, L., von Bloh, W., Brovkin, V., Cadule, P., Doney, S., Eby, M., Fung, I., Bala, G., John, J., Jones, C., Joos, F., Kato, T., Kawamiya, M., Knorr, W., Lindsay, K., Matthews, H. D., Raddatz, T., Rayner, P.,
465   Reick, C., Roeckner, E., Schnitzler, K.-G., Schnur, R., Strassmann, K., Weaver, A. J., Yoshikawa, C., and Zeng, N.: Climate–Carbon Cycle Feedback Analysis: Results from the C[4] MIP Model Intercomparison, J. Clim., 19, 3337–3353, https://doi.org/10.1175/JCLI3800.1, 2006.

Friedlingstein, P., Jones, M. W., O'Sullivan, M., Andrew, R. M., Hauck, J., Peters, G. P., Peters, W., Pongratz, J., Sitch, S., Le Quéré, C., Bakker, D. C. E., Canadell, J. G., Ciais, P., Jackson, R. B., Anthoni, P., Barbero, L., Bastos, A.,
470   Bastrikov, V., Becker, M., Bopp, L., Buitenhuis, E., Chandra, N., Chevallier, F., Chini, L. P., Currie, K. I., Feely, R. A., Gehlen, M., Gilfillan, D., Gkritzalis, T., Goll, D. S., Gruber, N., Gutekunst, S., Harris, I., Haverd, V., Houghton, R. A., Hurtt, G., Ilyina, T., Jain, A. K., Joetzjer, E., Kaplan, J. O., Kato, E., Klein Goldewijk, K., Korsbakken, J. I., Landschützer, P., Lauvset, S. K., Lefèvre, N., Lenton, A., Lienert, S., Lombardozzi, D., Marland, G., McGuire, P. C., Melton, J. R., Metzl, N., Munro, D. R., Nabel, J. E. M. S., Nakaoka, S.-I., Neill, C., Omar, A. M., Ono, T., Peregon, A., Pierrot, D., Poulter, B.,
475   Rehder, G., Resplandy, L., Robertson, E., Rödenbeck, C., Séférian, R., Schwinger, J., Smith, N., Tans, P. P., Tian, H., Tilbrook, B., Tubiello, F. N., van der Werf, G. R., Wiltshire, A. J., and Zaehle, S.: Global Carbon Budget 2019, Earth Syst. Sci. Data, 11, 1783–1838, https://doi.org/10.5194/essd-11-1783-2019, 2019.

Gelaro, R., McCarty, W., Suárez, M. J., Todling, R., Molod, A., Takacs, L., Randles, C. A., Darmenov, A., Bosilovich, M. G., Reichle, R., Wargan, K., Coy, L., Cullather, R., Draper, C., Akella, S., Buchard, V., Conaty, A., da Silva, A. M., Gu, W.,

480 Kim, G.-K., Koster, R., Lucchesi, R., Merkova, D., Nielsen, J. E., Partyka, G., Pawson, S., Putman, W., Rienecker, M., Schubert, S. D., Sienkiewicz, M., and Zhao, B.: The Modern-Era Retrospective Analysis for Research and Applications, Version 2 (MERRA-2), J. Clim., 30, 5419–5454, https://doi.org/10.1175/JCLI-D-16-0758.1, 2017.

Gruber, N., Clement, D., Carter, B. R., Feely, R. A., van Heuven, S., Hoppema, M., Ishii, M., Key, R. M., Kozyr, A., Lauvset, S. K., Lo Monaco, C., Mathis, J. T., Murata, A., Olsen, A., Perez, F. F., Sabine, C. L., Tanhua, T., and Wanninkhof, R.: The

485 oceanic sink for anthropogenic CO_2 from 1994 to 2007, Science, 363, 1193–1199, https://doi.org/10.1126/science.aau5153, 2019.

Gurney, K. R., Law, R. M., Denning, A. S., Rayner, P. J., Pak, B. C., Baker, D., Bousquet, P., Bruhwiler, L., Chen, Y.-H., Ciais, P., Fung, I. Y., Heimann, M., John, J., Maki, T., Maksyutov, S., Peylin, P., Prather, M., and Taguchi, S.: Transcom 3 inversion intercomparison: Model mean results for the estimation of seasonal carbon sources and sinks: T3 SEASONAL

490 RESULTS, Glob. Biogeochem. Cycles, 18, n/a-n/a, https://doi.org/10.1029/2003GB002111, 2004.

Hunt, B. R., Kostelich, E. J., and Szunyogh, I.: Efficient Data Assimilation for Spatiotemporal Chaos: a Local Ensemble Transform Kalman Filter, arXiv:physics/0511236, 2005.

Hunt, B. R., Kostelich, E. J., and Szunyogh, I.: Efficient data assimilation for spatiotemporal chaos: A local ensemble transform Kalman filter, Phys. Nonlinear Phenom., 230, 112–126, https://doi.org/10.1016/j.physd.2006.11.008, 2007.

495 Kalnay, E. and Yang, S.-C.: Accelerating the spin-up of Ensemble Kalman Filtering, Q. J. R. Meteorol. Soc., 136, 1644–1651, https://doi.org/10.1002/qj.652, 2010.

Kang, J.-S., Kalnay, E., Liu, J., Fung, I., Miyoshi, T., and Ide, K.: "Variable localization" in an ensemble Kalman filter: Application to the carbon cycle data assimilation, J. Geophys. Res., 116, D09110, https://doi.org/10.1029/2010JD014673, 2011.

500 Kang, J.-S., Kalnay, E., Miyoshi, T., Liu, J., and Fung, I.: Estimation of surface carbon fluxes with an advanced data assimilation methodology, J. Geophys. Res. Atmospheres, 117, D24101, https://doi.org/10.1029/2012JD018259, 2012.

Kondo, M., Patra, P. K., Sitch, S., Friedlingstein, P., Poulter, B., Chevallier, F., Ciais, P., Canadell, J. G., Bastos, A., Lauerwald, R., Calle, L., Ichii, K., Anthoni, P., Arneth, A., Haverd, V., Jain, A. K., Kato, E., Kautz, M., Law, R. M., Lienert, S., Lombardozzi, D., Maki, T., Nakamura, T., Peylin, P., Rödenbeck, C., Zhuravlev, R., Saeki, T., Tian, H., Zhu, D., and Ziehn,

505 T.: State of the science in reconciling top-down and bottom-up approaches for terrestrial CO_2 budget, Glob. Change Biol., 26, 1068–1084, https://doi.org/10.1111/gcb.14917, 2020.

Liu, J., Fung, I., Kalnay, E., and Kang, J.-S.: CO_2 transport uncertainties from the uncertainties in meteorological fields, Geophys. Res. Lett., 38, L12808, https://doi.org/10.1029/2011GL047213, 2011.

Liu, J., Fung, I., Kalnay, E., Kang, J.-S., Olsen, E. T., and Chen, L.: Simultaneous assimilation of AIRS Xco_2 and

510 meteorological observations in a carbon climate model with an ensemble Kalman filter: ASSIMILATION OF AIRS XCO_2, J. Geophys. Res. Atmospheres, 117, D05309, https://doi.org/10.1029/2011JD016642, 2012.

Liu, J., Bowman, K. W., Lee, M., Henze, D. K., Bousserez, N., Brix, H., James Collatz, G., Menemenlis, D., Ott, L., Pawson, S., Jones, D., and Nassar, R.: Carbon monitoring system flux estimation and attribution: impact of ACOS-GOSAT XCO_2

sampling on the inference of terrestrial biospheric sources and sinks, Tellus B Chem. Phys. Meteorol., 66, 22486,
515   https://doi.org/10.3402/tellusb.v66.22486, 2014.

Liu, Y., Kalnay, E., Zeng, N., Asrar, G., Chen, Z., and Jia, B.: Estimating surface carbon fluxes based on a local ensemble
transform Kalman filter with a short assimilation window and a long observation window: an observing system simulation
experiment test in GEOS-Chem 10.1, Geosci. Model Dev., 12, 2899–2914, https://doi.org/10.5194/gmd-12-2899-2019,
2019.

520   Lokupitiya, R. S., Zupanski, D., Denning, A. S., Kawa, S. R., Gurney, K. R., and Zupanski, M.: Estimation of global CO_2
fluxes at regional scale using the maximum likelihood ensemble filter, J. Geophys. Res., 113, D20110,
https://doi.org/10.1029/2007JD009679, 2008.

Mitchell, H. L. and Houtekamer, P. L.: An Adaptive Ensemble Kalman Filter, Mon. Weather Rev., 128, 416,
https://doi.org/10.1175/1520-0493(2000)128<0416:AAEKF>2.0.CO;2, 2000.

525   Miyoshi, T.: The Gaussian Approach to Adaptive Covariance Inflation and Its Implementation with the Local Ensemble
Transform Kalman Filter, Mon. Weather Rev., 139, 1519–1535, https://doi.org/10.1175/2010MWR3570.1, 2011.

Nassar, R., Napier-Linton, L., Gurney, K. R., Andres, R. J., Oda, T., Vogel, F. R., and Deng, F.: Improving the temporal and
spatial distribution of CO_2 emissions from global fossil fuel emission data sets, J. Geophys. Res. Atmospheres, 118, 917–
933, https://doi.org/10.1029/2012JD018196, 2013.

530   Oda, T. and Maksyutov, S.: A very high-resolution (1 km×1 km) global fossil fuel CO2 emission inventory derived using a
point source database and satellite observations of nighttime lights, Atmospheric Chem. Phys., 11, 543–556, 2011.

Pan, M. and Wood, E. F.: Data Assimilation for Estimating the Terrestrial Water Budget Using a Constrained Ensemble
Kalman Filter, J. Hydrometeorol., 7, 534–547, https://doi.org/10.1175/JHM495.1, 2006.

Peters, W., Miller, J. B., Whitaker, J., Denning, A. S., Hirsch, A., Krol, M. C., Zupanski, D., Bruhwiler, L., and Tans, P. P.:
535   An ensemble data assimilation system to estimate CO_2 surface fluxes from atmospheric trace gas observations, J. Geophys.
Res., 110, D24304, https://doi.org/10.1029/2005JD006157, 2005.

Peters, W., Jacobson, A. R., Sweeney, C., Andrews, A. E., Conway, T. J., Masarie, K., Miller, J. B., Bruhwiler, L. M. P.,
Petron, G., Hirsch, A. I., Worthy, D. E. J., van der Werf, G. R., Randerson, J. T., Wennberg, P. O., Krol, M. C., and Tans,
P. P.: An atmospheric perspective on North American carbon dioxide exchange: CarbonTracker, Proc. Natl. Acad. Sci., 104,
540   18925–18930, https://doi.org/10.1073/pnas.0708986104, 2007.

Rodenbeck, C., Houweling, S., Gloor, M., and Heimann, M.: CO_2 flux history 1982–2001 inferred from atmospheric data
using a global inversion of atmospheric transport, Atmospheric Chem. Phys., 3, 1919–1964, 2003.

Ruiz, J. J., Pulido, M., and Miyoshi, T.: Estimating Model Parameters with Ensemble-Based Data Assimilation: A Review, J.
Meteorol. Soc. Jpn. Ser II, 91, 79–99, https://doi.org/10.2151/jmsj.2013-201, 2013.

545   Sasakawa, M., Shimoyama, K., Machida, T., Tsuda, N., Suto, H., Arshinov, M., Davydov, D., Fofonov, A., Krasnov, O., Saeki,
T., Koyama, Y., and Maksyutov, S.: Continuous measurements of methane from a tower network over Siberia, Tellus B
Chem. Phys. Meteorol., 62, 403–416, https://doi.org/10.1111/j.1600-0889.2010.00494.x, 2010.

Schuh, A. E., Jacobson, A. R., Basu, S., Weir, B., Baker, D., Bowman, K., Chevallier, F., Crowell, S., Davis, K. J., Deng, F., Denning, S., Feng, L., Jones, D., Liu, J., and Palmer, P. I.: Quantifying the Impact of Atmospheric Transport Uncertainty

550   on CO_2 Surface Flux Estimates, Glob. Biogeochem. Cycles, 33, 484–500, https://doi.org/10.1029/2018GB006086, 2019.

Schuldt, K. N., Mund, J., Luijkx, I. T., Jacobson, A. R., Cox, A., Vermeulen, A., Manning, A., Beyersdorf, A., Manning, A., Karion, A., Hensen, A., Arlyn Andrews, Frumau, A., Colomb, A., Scheeren, B., Law, B., Baier, B., Munger, B., Paplawsky, B., Viner, B., Stephens, B., Daube, B., Labuschagne, C., Myhre, C. L., Hanson, C., Miller, C. E., Plass-Duelmer, C., Sloop, C. D., Sweeney, C., Kubistin, D., Goto, D., Jaffe, D., Say, D., Dinther, D. V., Bowling, D., Dickon Young, Weyrauch, D.,

555   Worthy, D., Dlugokencky, E., Gloor, E., Cuevas, E., Reyes-Sanchez, E., Hintsa, E., Kort, E., Morgan, E., Apadula, F., Francois Gheusi, Meinhardt, F., Moore, F., Vitkova, G., Chen, G., Bentz, G., Manca, G., Brailsford, G., Forster, G., Riris, H., Meijer, H., Matsueda, H., Huilin Chen, Levin, I., Lehner, I., Mammarella, I., Bartyzel, J., Abshire, J. B., Elkins, J. W., Levula, J., Jaroslaw Necki, Pichon, J. M., Peischl, J., Müller-Williams, J., Turnbull, J., Miller, J. B., Lee, J., Lin, J., Josep-Anton Morgui, DiGangi, J. P., Hatakka, J., Coletta, J. D., Holst, J., Kominkova, K., McKain, K., Saito, K., Aikin, K., Davis,

560   K., Thoning, K., Tørseth, K., Haszpra, L., Mitchell, L., Gatti, L. V., Emmenegger, L., Lukasz Chmura, Merchant, L., Sha, M. K., Delmotte, M., Fischer, M. L., Schumacher, M., Torn, M., Leuenberger, M., Steinbacher, M., et al.: Multi-laboratory compilation of atmospheric carbon dioxide data for the period 1957-2019; obspack_co2_1_GLOBALVIEWplus_v6.0_2020-09-11, https://doi.org/10.25925/20200903, 2020.

Tans, P. P., Fung, I. Y., and Taikahashi, T.: Observational Constraints on the Global Atmospheric CO2 Budget, Science, 9,

565   1990.

Whitaker, J. S. and Hamill, T. M.: Evaluating Methods to Account for System Errors in Ensemble Data Assimilation, Mon. Weather Rev., 140, 3078–3089, https://doi.org/10.1175/MWR-D-11-00276.1, 2012.

Whitaker, J. S., Hamill, T. M., Wei, X., Song, Y., and Toth, Z.: Ensemble Data Assimilation with the NCEP Global Forecast System, Mon. Weather Rev., 136, 463–482, https://doi.org/10.1175/2007MWR2018.1, 2008.

570   Wu, L., Bocquet, M., Chevallier, F., Lauvaux, T., and Davis, K.: Hyperparameter estimation for uncertainty quantification in mesoscale carbon dioxide inversions, Tellus B Chem. Phys. Meteorol., 65, 20894, https://doi.org/10.3402/tellusb.v65i0.20894, 2013.

Yang, D., Liu, Y., Cai, Z., Chen, X., Yao, L., and Lu, D.: First Global Carbon Dioxide Maps Produced from TanSat Measurements, Adv. Atmospheric Sci., 35, 621–623, https://doi.org/10.1007/s00376-018-7312-6, 2018.

575   Yokota, T., Yoshida, Y., Eguchi, N., Ota, Y., Tanaka, T., Watanabe, H., and Maksyutov, S.: Global Concentrations of CO2 and CH4 Retrieved from GOSAT: First Preliminary Results, SOLA, 5, 160–163, https://doi.org/10.2151/sola.2009-041, 2009.

Zeng, N., Mariotti, A., and Wetzel, P.: Terrestrial mechanisms of interannual CO_2 variability, Glob. Biogeochem. Cycles, 19, https://doi.org/10.1029/2004GB002273, 2005.

580   Zeng, Y., Janjić, T., Ruckstuhl, Y., and Verlaan, M.: Ensemble-type Kalman filter algorithm conserving mass, total energy and enstrophy: SQPEns Conserving Mass, Total Energy and Enstrophy, Q. J. R. Meteorol. Soc., 143, 2902–2914,

https://doi.org/10.1002/qj.3142, 2017.

Zhang, F., Snyder, C., and Sun, J.: Impacts of Initial Estimate and Observation Availability on Convective-Scale Data Assimilation with an Ensemble Kalman Filter, Mon. Weather Rev., 132, 16, 2004.

585   Zupanski, D., Denning, A. S., Uliasz, M., Zupanski, M., Schuh, A. E., Rayner, P. J., Peters, W., and Corbin, K. D.: Carbon flux bias estimation employing Maximum Likelihood Ensemble Filter (MLEF), J. Geophys. Res., 112, D17107, https://doi.org/10.1029/2006JD008371, 2007.